

# Fourteen new eclipsing white dwarf plus main-sequence binaries from the SDSS and Catalina surveys

S. G. Parsons<sup>1\*</sup>, C. Agurto-Gangas<sup>1</sup>, B. T. Gänsicke<sup>2</sup>, A. Rebassa-Mansergas<sup>3</sup>,  
M. R. Schreiber<sup>1,4</sup>, T. R. Marsh<sup>2</sup>, V. S. Dhillon<sup>5</sup>, S. P. Littlefair<sup>5</sup>, A. J. Drake<sup>6</sup>,  
M. C. P. Bours<sup>2</sup>, E. Breedt<sup>2</sup>, C. M. Copperwheat<sup>7</sup>, L. K. Hardy<sup>5</sup>, C. Buisset<sup>8</sup>,  
P. Prasić<sup>8</sup> and J. J. Ren<sup>9</sup>

<sup>1</sup> *Departamento de Física y Astronomía, Universidad de Valparaíso, Avenida Gran Bretaña 1111, Valparaíso, Chile*

<sup>2</sup> *Department of Physics, University of Warwick, Coventry CV4 7AL, UK*

<sup>3</sup> *Kavli Institute for Astronomy and Astrophysics, Peking University, Beijing 100871, China*

<sup>4</sup> *Millennium Nucleus "Protoplanetary Disks in ALMA Early Science", Universidad de Valparaíso, Valparaíso 2360102, Chile*

<sup>5</sup> *Department of Physics and Astronomy, University of Sheffield, Sheffield, S3 7RH, UK*

<sup>6</sup> *California Institute of Technology, 1200 E. California Blvd, CA 91225, USA*

<sup>7</sup> *Astrophysics Research Institute, Liverpool John Moores University, Liverpool L3 5RF, UK*

<sup>8</sup> *National Astronomical Research Institute of Thailand, 191 Siriphanich Building, Huay Kaew Road, Chiang Mai 50200, Thailand*

<sup>9</sup> *Department of Astronomy, Peking University, Beijing 100871, P. R. China*

Accepted 2015 February 18. Received 2015 February 17; in original form 2015 February 2

## ABSTRACT

We report on the search for new eclipsing white dwarf plus main-sequence (WDMS) binaries in the light curves of the Catalina surveys. We use a colour selected list of almost 2000 candidate WDMS systems from the Sloan Digital Sky Survey, specifically designed to identify WDMS systems with cool white dwarfs and/or early M type main-sequence stars. We identify a total of 17 eclipsing systems, 14 of which are new discoveries. We also find 3 candidate eclipsing systems, 2 main-sequence eclipsing binaries and 22 non-eclipsing close binaries. Our newly discovered systems generally have optical fluxes dominated by the main-sequence components, which have earlier spectral types than the majority of previously discovered eclipsing systems. We find a large number of ellipsoidally variable binaries with similar periods, near 4 hours, and spectral types M2–3, which are very close to Roche-lobe filling. We also find that the fraction of eclipsing systems is lower than found in previous studies and likely reflects a lower close binary fraction among WDMS binaries with early M-type main-sequence stars due to their enhanced angular momentum loss compared to fully convective late M type stars, hence causing them to become cataclysmic variables quicker and disappear from the WDMS sample. Our systems bring the total number of known detached, eclipsing WDMS binaries to 71.

**Key words:** binaries: close – binaries: eclipsing – stars: white dwarfs – stars: low mass

## 1 INTRODUCTION

The majority of main-sequence star binaries ( $\sim 75\%$ ) are sufficiently well separated that their stellar components can evolve independently of each other and effectively as single stars. The remaining  $\sim 25\%$  have separations small enough that when the more massive member of the binary ascends the giant branch, the two stars will interact with each other causing mass transfer via Roche-lobe overflow (Willems & Kolb 2004). This interaction often leads to a common envelope phase, during which the two stars orbit within a

single envelope of material, quickly losing angular momentum and spiraling towards each other (Webbink 1984; Ivanova et al. 2013). The result of this phase is a compact binary with a period of hours to days, comprised of the core of the initially more massive star and its main-sequence companion, known as a post common envelope binary (PCEB).

The most abundant type of PCEB are those containing a white dwarf with a low-mass main-sequence star companion. In recent years the number of these systems known has rapidly increased, thanks mainly to the Sloan Digital Sky Survey (SDSS; York et al. 2000; Adelman-McCarthy et al. 2008; Abazajian et al. 2009). The number of white dwarf plus main-sequence binaries (WDMS)

\* steven.parsons@uv.cl

**Table 1.** Journal of photometric observations. The eclipse of the white dwarf occurs at phase 0, 1 etc.

Target	Date at start of run	Telescope & instrument	Filter(s)	Start (UT)	Orbital phase	Exposure time (s)
SDSS J002412.87+174531.4	2013/07/09	LT+RISE	V+R	04:19	0.92 – 1.06	10.0
SDSS J042012.78+333739.7	2014/03/05	WHT+ULTRACAM	$u'g'r'$	20:15	0.79 – 1.06	5.2
SDSS J101356.32+272410.6	2012/12/19	LT+RISE	V+R	04:04	0.92 – 1.14	6.0
SDSS J112308.40+115559.3	2014/01/28	TNT+ULTRASPEC	KG5	17:19	0.92 – 1.04	7.8
SDSS J141150.74+211750.0	2013/05/12	LT+RISE	V+R	01:56	0.96 – 1.08	10.0
SDSS J141724.36+080112.0	2014/06/18	INT+WFC	$g$	22:59	0.91 – 1.09	20.0
SDSS J142427.69+112457.9	2013/04/22	WHT+ULTRACAM	$u'g'r'$	23:29	0.92 – 1.03	2.2
SDSS J154057.27+370543.4	2014/03/27	LT+RISE	V+R	04:00	0.88 – 1.11	10.0
SDSS J164235.97+063439.7	2014/04/22	LT+RISE	V+R	03:53	0.91 – 1.08	10.0
SDSS J220504.50+062248.6	2012/09/10	WHT+ULTRACAM	$u'g'r'$	23:00	0.80 – 1.07	3.1
SDSS J230627.54+055533.2	2015/01/02	TNT+ULTRASPEC	KG5	12:16	0.85 – 1.09	4.1

spectroscopically observed within SDSS has reached 2316 as of data release 8 (Rebassa-Mansergas et al. 2013a), with an additional 227 recently discovered in data release 9 (Li et al. 2014). From this large sample more than 200 close PCEB systems have been identified (Nebot Gómez-Morán et al. 2011; Parsons et al. 2013b). These systems have been used to investigate many aspects of close binary evolution, such as disrupted magnetic braking (Schreiber et al. 2010), the common envelope efficiency (Zorotovic et al. 2010), the origin of low-mass white dwarfs (Rebassa-Mansergas et al. 2011) and activity in rapidly rotating M dwarfs (Rebassa-Mansergas et al. 2013b). Additional surveys are also adding to these numbers (e.g. the LAMOST surveys, Ren et al. 2014).

However, one limitation of the SDSS WDMS sample is that it is biased towards systems containing M dwarf stars with late spectral types and relatively hot white dwarfs. This is because the white dwarfs in these systems contribute a relatively large fraction of the optical flux, thus making their spectral features visible (hence easier to detect) and altering the colours of the objects sufficiently to move them well off the main-sequence, hence making these types of WDMS systems easier to identify. Moreover, the similar colours of WDMS of this type to quasars, which were specifically targeted within the SDSS spectroscopic survey, meant that these systems are overrepresented within the spectroscopic sample. WDMS binaries containing early-M or more massive main-sequence components and cooler white dwarfs generally have optical fluxes dominated by the main-sequence star making their identification as WDMS systems difficult, although 251 systems of this type were identified within the Sloan Extension for Galactic Understanding and Exploration (SEGUE) survey (Rebassa-Mansergas et al. 2012).

Eclipsing PCEBs are particularly useful since the eclipse allows us to directly measure the physical parameters of the binary virtually independent of model atmosphere calculations and hence test mass-radius relationships (Parsons et al. 2010a, 2012a,b; Pyrzas et al. 2012; Littlefair et al. 2014). Moreover, the sharp white dwarf eclipse features lead to extremely precise timing measurements and have led to the discovery of quasi-sinusoidal variations in the eclipse arrival times of many of these systems (Parsons et al. 2010b; Backhaus et al. 2012) which, in some cases, have been interpreted as the gravitational influence of circumbinary planets (Beuermann et al. 2010, 2012a,b; Marsh et al. 2014).

Recently Rebassa-Mansergas et al. (2013a) used a photometric selection criteria specifically designed to target WDMS systems in the SDSS dominated by the contribution from the main-sequence star, hence systems containing early type M dwarfs and/or cool white dwarfs. In this paper we combine this photometric catalogue

with data from the Catalina Sky Survey (CSS) and Catalina Real Time Transient Survey (CRTS; Drake et al. 2009) in order to search for new eclipsing systems. We also provide a full list of known detached, eclipsing white dwarf plus main-sequence / brown dwarf binaries published to date.

## 2 SAMPLE SELECTION AND DATA REDUCTION

We use the list of 3419 photometrically selected white dwarf plus main-sequence binary candidates from Rebassa-Mansergas et al. (2013a). These were selected based on a combination of optical (SDSS) and infrared (UKIRT, 2MASS and WISE) colours. The catalogue also contains 47 spectroscopically confirmed white dwarf plus main-sequence binaries from SDSS DR 8. We select those systems with magnitudes of  $g < 19$  and CSS coverage, resulting in a total sample of 2060 systems.

We re-reduced the raw CSS data ourselves using the method outlined in Parsons et al. (2013b), which allowed us to more easily identify deeply eclipsing systems as well as remove any contaminated exposures. Some of our objects were completely blended with nearby stars and so we remove these from our sample. In total we had 1958 objects with good CSS photometry.

## 3 FOLLOW-UP DATA

We obtained follow-up photometry and spectroscopy for a number of our systems. In this section we outline those observations and their reduction. Unfortunately, due to limited observing time, we have been unable to obtain follow-up high-speed photometry for 3 of the new eclipsing systems. A full summary of the photometric observations is given in Table 1.

### 3.1 William Herschel Telescope + ULTRACAM photometry

We observed three of our new eclipsing systems with the high speed frame-transfer camera ULTRACAM (Dhillon et al. 2007) mounted as a visitor instrument on the 4.2-m William Herschel Telescope (WHT) on La Palma. The observations targeted the eclipse of the white dwarf. ULTRACAM uses a triple beam setup allowing one to obtain data in three separate bands simultaneously with a deadtime between frames of only 24 milliseconds. For all of our observations we used ULTRACAM equipped with  $u'$ ,  $g'$  and  $r'$  filters.

All of these data were reduced using the ULTRACAM

**Table 2.** Journal of NAOC+BFOSC spectroscopic observations.

Target	Date at start of run	UT (mid-exposure)	Exposure time (mins)
SDSS J0031+2634	2014/08/06	20:04	25
SDSS J0046-0339	2014/08/06	19:33	25
SDSS J0054+1429	2014/08/06	19:07	35
SDSS J0249+0713	2014/08/04	20:08	20
SDSS J1411+2117	2014/08/07	13:19	25
SDSS J1506+2152	2014/08/06	13:31	30
SDSS J1540+3705	2014/08/06	15:05	25
SDSS J2053+0015	2014/08/04	16:31	20
SDSS J2122+1039	2014/08/06	15:56	35
SDSS J2148+1927	2014/08/06	14:34	40
SDSS J2205-0622	2014/08/04	19:47	45
SDSS J2229+1853	2014/08/04	17:51	30
SDSS J2241+2536	2014/08/04	17:11	25
SDSS J2256+1822	2014/08/04	18:50	40
SDSS J2327+2119	2014/08/06	17:01	40
SDSS J2339+1157	2014/08/06	18:20	30
SDSS J2340+1855	2014/08/06	17:47	35

pipeline software (Dhillon et al. 2007). Debiassing, flatfielding and sky background subtraction were performed in the standard way. The source flux was determined with aperture photometry using a variable aperture, whereby the radius of the aperture is scaled according to the full width at half maximum (FWHM). Variations in observing conditions were accounted for by determining the flux relative to a comparison star in the field of view.

### 3.2 Liverpool Telescope + RISE photometry

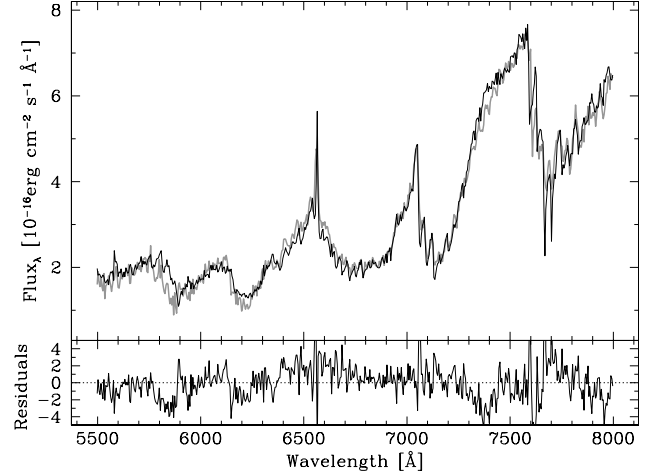
We used the high speed camera RISE (Steele et al. 2008) on the Liverpool Telescope (LT) to observe the eclipses of five of our systems. RISE is a frame transfer CCD camera with a single wide-band V+R filter and negligible downtime between frames. The raw data are automatically run through a pipeline that debiases, removes a scaled dark frame and flat-fields the data. We used the ULTRACAM pipeline to perform aperture photometry on the RISE data in the same way as described in the previous section.

### 3.3 Thai National Telescope + ULTRASPEC photometry

Two of our eclipsing systems were observed with the high-speed ULTRASPEC camera (Dhillon et al. 2014) mounted on the 2.4-m Thai National Telescope (TNT), located on Doi Inthanon, Thailand. ULTRASPEC has a frame transfer EMCCD with a downtime between exposures of 15 milliseconds. Our observations were designed to cover the white dwarf eclipses. We used the Schott KG5 filter, which is a broad filter with a central wavelength of 5075Å and FWHM of 3605Å and hence covers the  $u'$ ,  $g'$  and  $r'$  bandpasses. We again used the ULTRACAM pipeline to reduce the data.

### 3.4 Isaac Newton Telescope + WFC photometry

We observed one of our new eclipsing systems with the Wide Field Camera (WFC) mounted at the prime focus of the 2.5-m Isaac Newton Telescope (INT) on La Palma. The observations were performed with the Sloan-Gunn  $g$  filter and we windowed the detector in order to reduce the read-out time to  $\sim 2$  seconds. Once again the ULTRACAM pipeline was used to reduce the data.

**Figure 1.** BFOSC Spectrum of one of our newly identified PCEB systems (SDSS J2241+2536, gray line) with the best fit template spectrum overplotted (black line). The lower panel shows the residuals of the fit.

### 3.5 NAOC Xinglong + BFOSC spectroscopy

Low-resolution spectroscopic observations of 17 targets showing variation in their light curves were performed with the 2.16-m optical telescope at the Xinglong Station of the National Astronomical Observatories, Chinese Academy of Sciences (NAOC), using the BAO Faint Object Spectrograph and Camera (BFOSC). The observations were performed in August 2014 and we covered as many close systems (both eclipsing and non-eclipsing) as were visible at the time. We used the low resolution grism-G5 with a dispersion degree of 1.99 Å/mm, a spectral resolution of 2.98Å and a long-slit of width 1.8". The spectra cover the wavelength range of 5200Å–10120Å. The typical seeing varied from 1.8" to 3.0". A summary of these observations is given in Table 2.

The spectroscopic data were reduced following the grating spectroscopy procedures provided in the PAMELA and MOLLY<sup>1</sup> packages. The spectra were first bias subtracted and flat-fielded, then the object spectra were optimally extracted. The wavelength calibration was performed with Fe/Ar lamps exposed at the beginning and the end of each night. The observations of spectral standard stars were used to flux calibrate and remove the telluric features from our spectra.

The spectra were substantially affected by fringing. This effect was particularly pronounced at wavelengths beyond 8000Å, therefore we only used the reliable range of 5500Å–8000Å for determining the spectral types of the main-sequence stars. Since the main-sequence stars dominate over the white dwarfs in all our spectra we are unable to place any constraints on the white dwarf parameters. We determined the spectral types of the main-sequence stars using the technique outlined in Rebassa-Mansergas et al. (2007), these are listed in Table 3 and Table A1 with an uncertainty of  $\pm 1$  class. An example fit is shown in Figure 1.

<sup>1</sup> PAMELA and MOLLY are available from [www2.warwick.ac.uk/fac/sci/physics/research/astro/people/marsh/software](http://www2.warwick.ac.uk/fac/sci/physics/research/astro/people/marsh/software)

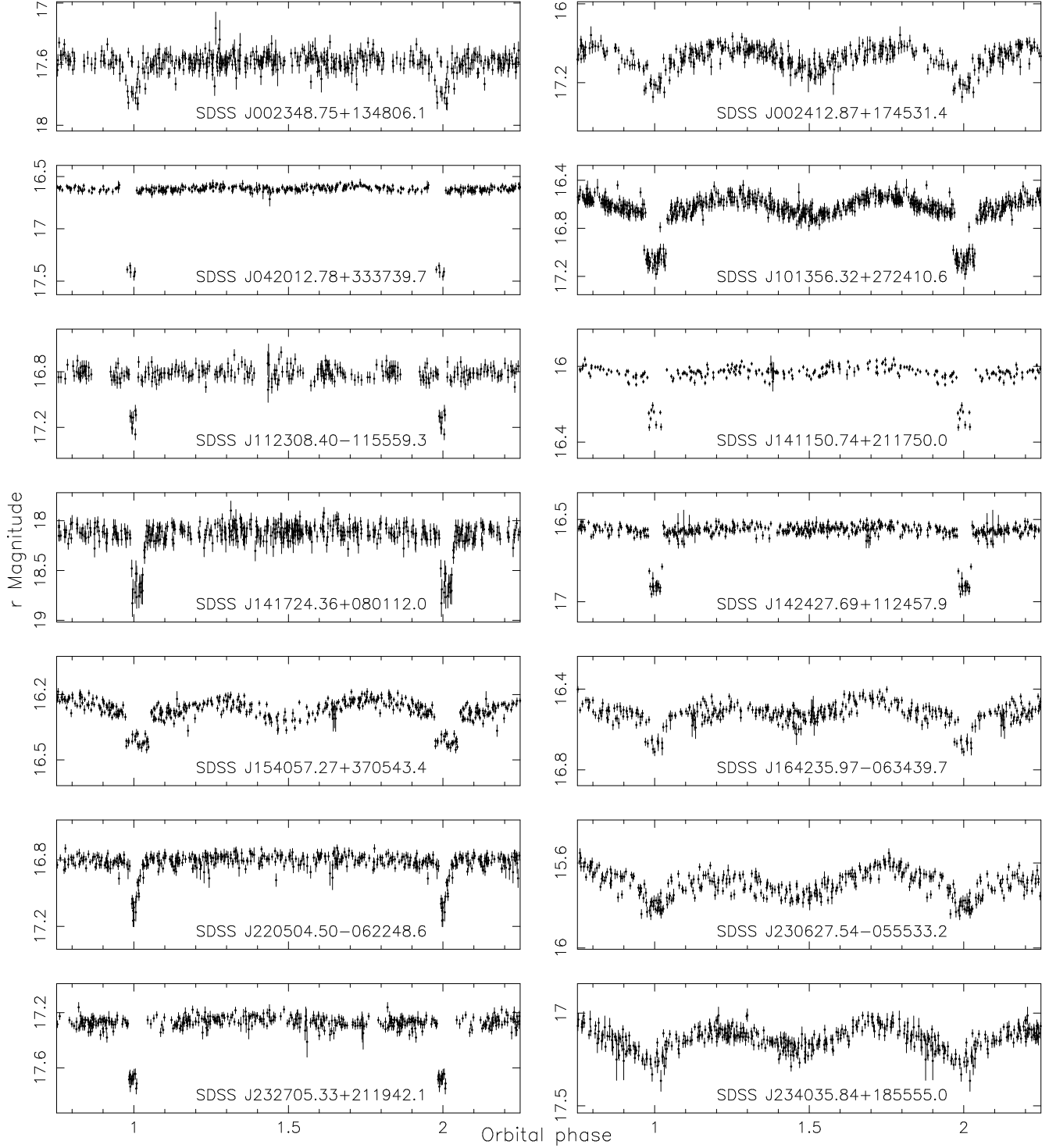


**Figure 2.** Phase-folded CSS light curves of the 14 newly identified eclipsing PCEBs. SDSS J234035.84+185555.0 is a marginal detection and requires some follow-up data to confirm the eclipse.

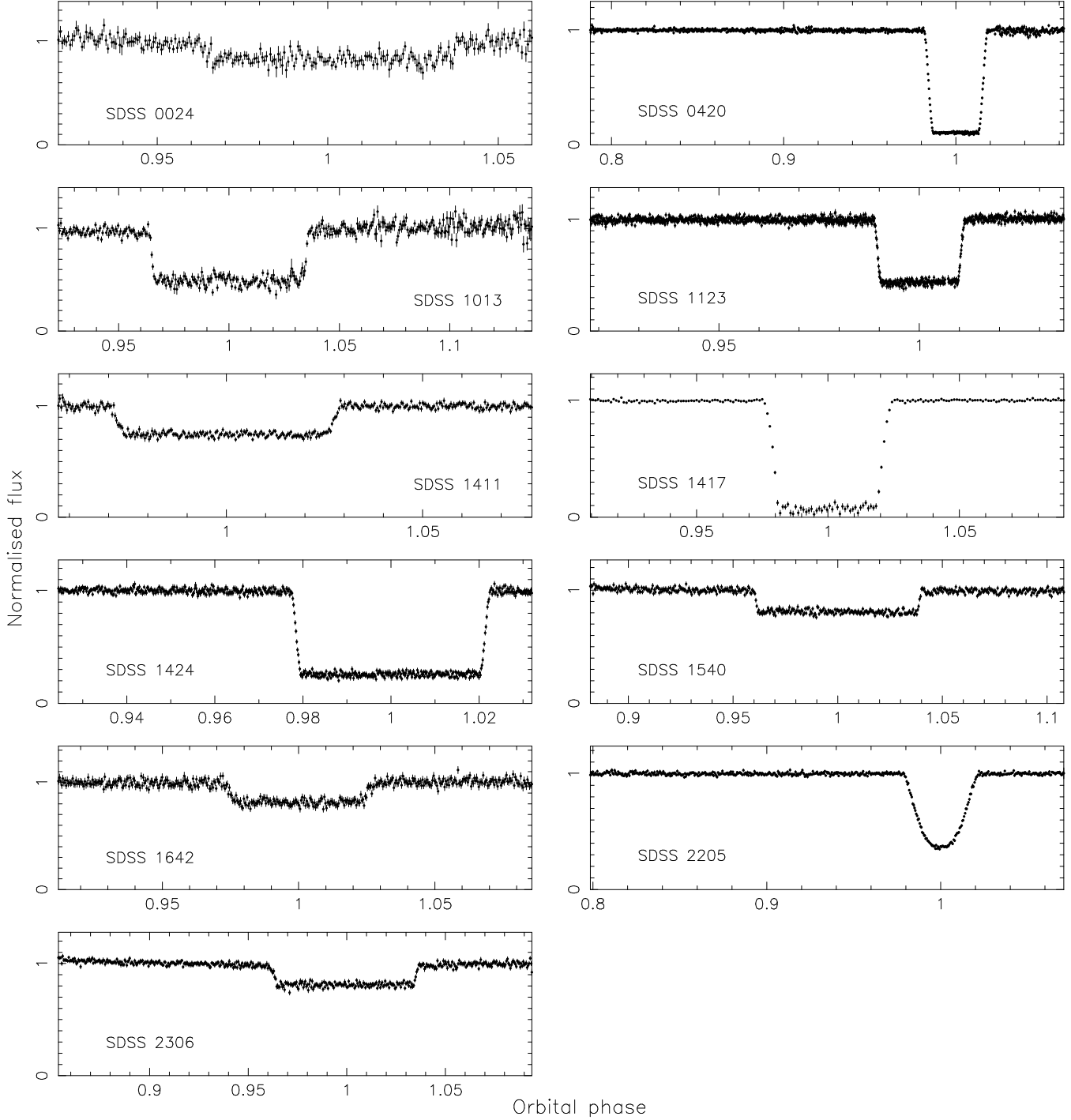


**Figure 3.** Follow-up light curves of 11 of the newly identified eclipsing systems, see Table 1 for the telescope+instrument+filter used for each observation. In the case of multiple bands we have plotted the  $g'$  band eclipse.

#### 4 RESULTS

We search for periodic signals in each of our 1958 CSS light curves using several different period finding algorithms. We used a combination of Lomb-Scargle (Scargle 1982) and an analysis of variance period search on the light curves using a multi-harmonic model (Schwarzenberg-Czerny 1996), as well as phase dispersion minimisation (Stellingwerf 1978). These latter two approaches are more sensitive to shallow eclipse features. We then used these results to

identify eclipsing systems, as well as any other periodically variable systems (i.e. reflection effects and ellipsoidal variations). Finally, we also used a simplified version of the Box-Fitting Least Squares method (Kovács et al. 2002), described in more detail in Parsons et al. (2013b)

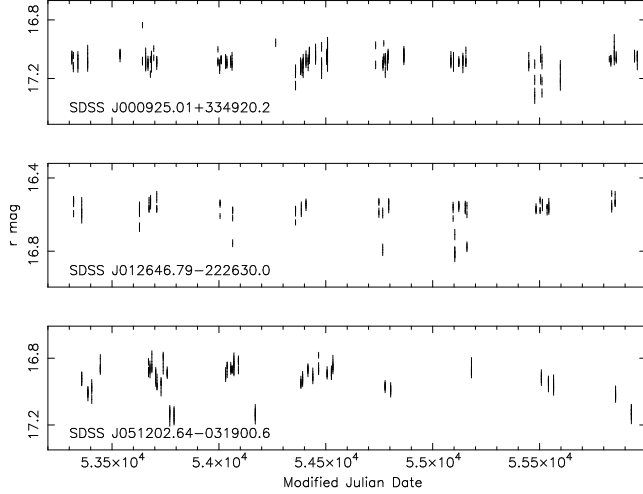


**Figure 4.** CSS light curves of the three candidate eclipsing WDMS systems. All show several fainter points indicative of an eclipse, but no obvious periodicity is found. More data are needed to determine their periods.

#### 4.1 New eclipsing systems

From our analysis we have identified a total of 17 eclipsing systems, 14 previously unknown systems and 3 systems that were already known to be eclipsing PCEBs: WD 1333+005 (Drake et al. 2010), CSS J0314+0206 (Drake et al. 2014a) and CSS J0935+2700 (Drake et al. 2014b). For 11 of these 14 new systems we have obtained high-speed photometry of the eclipse of the white dwarf. We list the details of these eclipsing systems, along with all other known eclipsing white dwarf plus main-sequence / brown dwarf binaries (a total of 71) in Table A1, in the appendix. The phase-folded CSS light curves are shown in Figure 2 and our follow-up high-speed photometry of the white dwarf eclipses are shown in Figure 3. The majority of the new eclipsing systems show shallow eclipses ( $<0.5$  mag) and large ellipsoidal modulation. We discuss some of the more interesting systems in more detail in Section 5.4.

Along with these new eclipsing systems, we identify three additional eclipsing WDMS candidate systems. SDSS J000925.01+334920.2, SDSS J012646.79+222630.0 and SDSS J051202.64+031900.6 all show a number of faint points in their light curves. However, none of them show any convincing periodic signals. We show their CSS light curves in Figure 4. We also identify SDSS J023311.75+064112.8 and SDSS J170007.60+153425.5 as eclipsing main-sequence plus main-sequence binaries, as revealed by the presence of deep secondary eclipses, with periods of 0.5212d and 2.0482d respectively. We show their phase-folded light curves in Figure 5.

#### 4.2 Non-eclipsing systems

As well as eclipsing systems we also discovered 22 objects with periodically varying light curves caused either by irradiation effects or the distorted shape of the main-sequence star, known as ellipsoidal modulation. These are detailed in Table 3. Eight of these have previously been identified as close binaries by Drake et al. (2014a,b), our measured periods are consistent with theirs. None of these light curves showed any obvious eclipse features. However, as noted in Parsons et al. (2013b), systems that display large ellipsoidal amplitudes are likely to also have high inclinations. Therefore, it is likely that some of these may also be eclipsing, but the eclipse is too shallow to be detected in the CSS photometry. This is demonstrated in

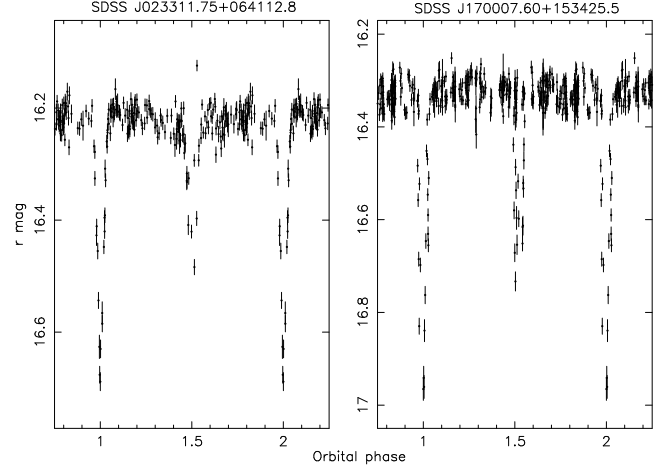


**Figure 5.** Phase-folded CSS light curves of the two newly identified eclipsing main-sequence plus main-sequence binaries.

**Table 3.** Non-eclipsing variables showing ellipsoidal modulation (E) or reflection effects (R). We also list the amplitude of the variation and the spectroscopically measured spectral type of the main-sequence star in the binary (with an uncertainty of  $\pm 1$  class) for those with spectra. The systems highlighted in bold were previously discovered by Drake et al. (2014a).

Object	Period (days)	Amp (mags)	Spectral type	Type
SDSS J003159.53+263445.7	0.23857749	0.092	M2	E
<b>SDSS J004638.02+033908.3</b>	0.17490842	0.210	M2	E
SDSS J005400.33+142931.2	0.17178094	0.205	M3	E
SDSS J024924.76+071344.2	0.17333085	0.234	M2	E
<b>SDSS J075015.11+494333.2</b>	0.17300847	0.152	-	E
SDSS J081437.77+425236.6	0.21221388	0.046	-	E
<b>SDSS J083405.20+300039.8</b>	0.26143431	0.122	-	E
SDSS J083947.39+022332.0	0.10758061	0.117	-	E
<b>SDSS J085414.28+211148.2</b>	0.20430622	0.156	-	E
<b>SDSS J090119.23+114255.1</b>	0.18668802	0.256	-	E
SDSS J122942.09+105732.9	0.16602091	0.084	-	E
SDSS J135048.24+124630.8	0.81625256	0.068	-	E
<b>SDSS J150606.71+215246.0</b>	0.18594902	0.232	M3	E
SDSS J205321.72+001536.3	0.17897014	0.141	M3	E
SDSS J212244.75+103915.2	0.18130918	0.147	M3	E
SDSS J214857.39+192759.7	0.18455907	0.092	M4	R
<b>SDSS J222918.95+185340.2</b>	0.18918441	0.248	M3	E
<b>SDSS J224134.90+253648.6</b>	0.15737950	0.296	M4	E
SDSS J225428.64+131528.6	0.38236318	0.079	-	E
SDSS J225607.11+182245.6	0.16377587	0.206	M3	E
SDSS J233900.39+115707.2	0.12286761	0.148	M5	E
SDSS J235320.09+141532.5	0.15181691	0.120	-	E

low to be detected in the CSS photometry. This is demonstrated in Figure 6, which shows a  $g'$  band light curve of SDSS J0745+2631, a binary that displays large ellipsoidal modulation (0.254 mags) in its CSS light curve previously discovered in the SDSS spectroscopic sample by Parsons et al. (2013b). In that paper we were unable to confirm its eclipsing nature because the eclipse is too shallow at the wavelengths of CSS and the LT follow-up photometry that was obtained. However, as Figure 6 shows, recently obtained ULTRACAM  $g'$  band shorter wavelength data reveals the presence of a shallow eclipse, confirming that systems showing large ellipsoidal modulation are likely to have at least shallow eclipses.

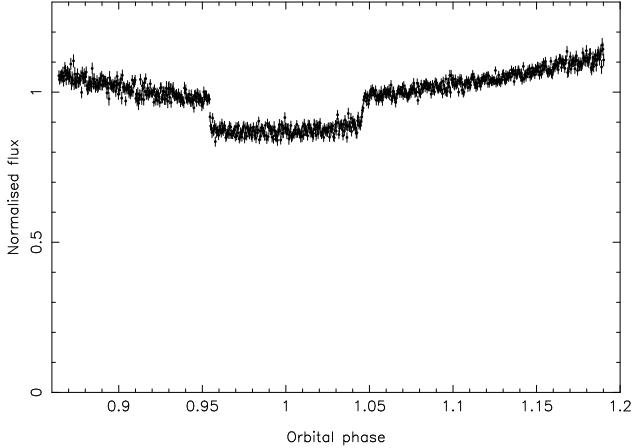


**Figure 6.** High-speed ULTRACAM  $g'$  band light curve of the eclipsing binary SDSS J0745+2631. This system was classified as an eclipsing “candidate” system by Parsons et al. (2013b) (it was not part of our photometric sample) because no eclipse could be detected in both the CSS photometry and the LT follow-up photometry. Shorter wavelength photometry was required to confirm the eclipse, which was expected based on the large amplitude of the ellipsoidal modulation in the CSS light curve. Many of the systems listed in Table 3 show very similar CSS light curves to this system and hence could also be eclipsing.

Two of the close binaries listed in Table 3 have slightly odd light curves, which are shown in Figure 7. In both cases there is a sinusoidal variation on half the orbital period, similar to ellipsoidal modulation, but one peak is much stronger than the other, similar to the O’Connell effect (O’Connell 1951). This effect is often seen in PCEBs with large Roche-lobe filling factors (Gänsicke et al. 2004; Tappert et al. 2007), but is not usually as stable on such long timescales. This could be accomplished by having a large star spot on one side of the main-sequence star, but it would have had to have persisted for the 8 years of CSS coverage, which is extremely unlikely. Further data is needed to properly understand the nature of these systems. The unusual light curve of SDSS J222918.95+185340.2 was previously noted by Drake et al. (2014a), as an example of a difficult to classify light curve.

## 5 DISCUSSION

### 5.1 Comparison with the spectroscopic sample

Figure 8 shows the colours of our newly discovered eclipsing and ellipsoidal binaries compared to the SDSS spectroscopic sample (Rebassa-Mansergas et al. 2012). Generally our newly discovered systems have much redder colours than the eclipsing systems from the spectroscopic sample, indicating that they contain cooler white dwarfs and/or earlier spectral type main-sequence stars, as confirmed from our spectroscopic observations and as expected from the colour selection itself (Rebassa-Mansergas et al. 2013a). This is because the colour cut was designed to carefully select WDMS systems whilst removing as much contamination as possible. This required good 2MASS and WISE infrared data (to remove quasars), which therefore selects against very late-type M stars, since they are usually too faint to have good infrared photometry.

For the spectroscopic WDMS sample  $\sim 1/3$  are thought to be close PCEBs (Schreiber et al. 2010; Rebassa-Mansergas et al. 2011), of which  $\sim 10\%$  are eclipsing (Parsons et al. 2013b). How-

ever, from our 1958 objects we only found 17 eclipsing systems, which is a much lower fraction than the spectroscopic sample (we would have expected  $\sim 60$  eclipsing systems). Assuming that the same fraction of close systems in our sample are eclipsing, this implies that the close binary fraction in the colour selected sample is only  $\sim 10\%$ . Even if all 21 of the ellipsoidal systems are in fact eclipsing (but not detectable in the CSS data), the fraction is still well below that of the spectroscopic sample.

There are three factors that contribute to this lower fraction. Firstly, as evidenced by our detection of 2 eclipsing main-sequence plus main-sequence binaries, the photometric sample is not pure, there is some contamination. Rebassa-Mansergas et al. (2013a) estimated that 84 per cent of the sample were very likely genuine WDMS systems, which is consistent with our finding 2 non-WDMS eclipsing systems compared to 17 WDMS eclipsers. However, even taking this contamination into account, the number of eclipsing systems is still well below that of the spectroscopic sample. Secondly, as previously noted, the colour selected sample contains systems with cooler white dwarfs and/or early M-type main-sequence stars. Therefore, the eclipse of the white dwarf is much shallower than the majority of those in the spectroscopic sample and hence some eclipsing systems may have been missed due to their eclipses not being detected in the CSS data (see the next section). Finally, Schreiber et al. (2010) found that within the spectroscopic sample the close binary fraction drops as one moves towards earlier type M stars. They interpret this as evidence of different angular momentum loss rates for different spectral types and therefore evidence of disrupted magnetic braking, since binaries containing these partially convective stars lose angular momentum much faster than their fully convective counterparts, and hence become cataclysmic variables much faster and disappear from the sample. In fact, Schreiber et al. (2010) found that the close binary fraction of WDMS systems with main-sequence stars of M2–3 spectral type is  $\sim 10\%$ , hence our results are fully consistent with the spectroscopic sample, and further support the idea of a spectral type dependent angular momentum loss rate.

### 5.2 Completeness

In order to better understand the low PCEB fraction of the photometric WDMS sample compared to the spectroscopic one, we have simulated CRTS light curves of the expected PCEB population within the photometric sample to see what percentage of systems should be detectable from their CRTS light curves and what parameters most affect this.

This was achieved by using the  $u - g$  colour of each object to predict the temperature of the white dwarf and main-sequence star spectral type using the constraints from Figure 4 of Rebassa-Mansergas et al. (2013a). We then used the mass-spectral type relation of Baraffe & Chabrier (1996) and mass-radius relationship of Morales et al. (2010) to determine the radius of the main-sequence star, which we consider to be the volume-averaged radius of the star.

We then randomly generated white dwarf masses and periods based on the distributions found from the spectroscopic PCEB sample (Zorotovic et al. 2011; Nebot Gómez-Morán et al. 2011). Random inclinations were also generated. Roche distortion was then applied to the main-sequence stars and light curves generated using a code specifically designed to simulate close binaries containing white dwarfs (see Copperwheat et al. 2010 for more details on the light curve code). The light curves were sampled at the times corresponding to the CRTS observations, and with the same photo-

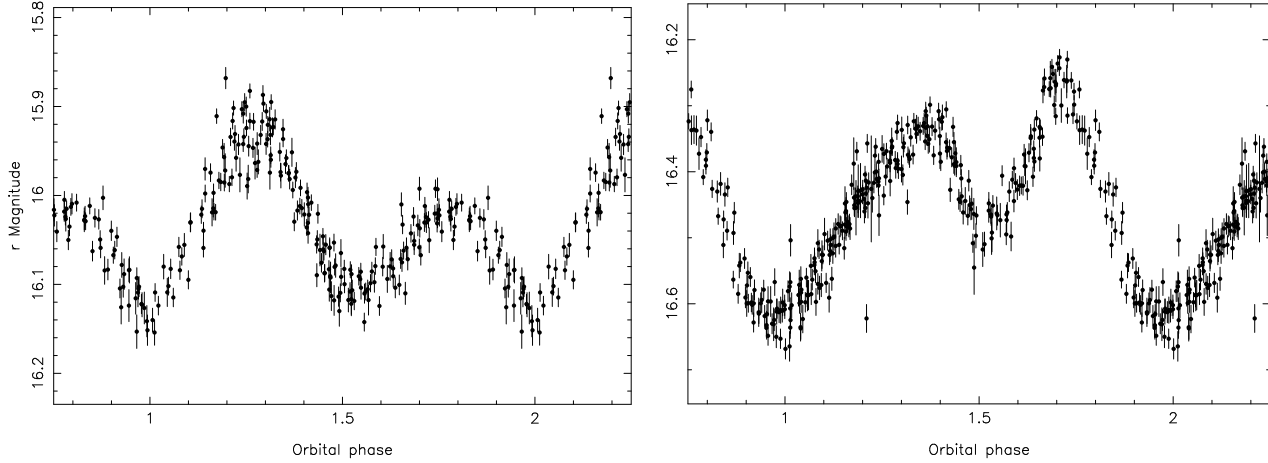


**Figure 7.** CSS light curves of SDSS J075015.11+494333.2 (left) and SDSS J222918.95+185340.2 (right). Both systems show variations similar to ellipsoidal modulation, but in both cases one maxima is lower than the other and for SDSS J222918.95+185340.2 the minima is substantially lower at phase 1.

metric uncertainties. Finally, we ran our period search algorithms on the resulting synthetic light curves and considered a PCEB successfully detected if the correct period was returned (or half the period, to account for ellipsoidal modulation systems).

The result of this simulation was that  $\sim 13.5\%$  of PCEBs should have been detectable from their CRTS light curves, of these  $\sim 40\%$  are eclipsing. The vast majority ( $\sim 95\%$ ) of the non-eclipsing systems were detected from ellipsoidal variations, the rest were detected from reflection effects, consistent with the results from Table 3. Figure 9 shows the chance of detecting a PCEB (success rate) as a function of the orbital period and main-sequence star mass. It is clear that the closer to Roche-lobe filling the star is, the higher the detection probability, since this leads to larger ellipsoidal modulation. The success rate drops substantially at periods of more than 0.5 days, with essentially only eclipsing systems being detected at these longer periods, consistent with our results.

If 13.5% of PCEBs within the photometric sample are detectable from their CRTS light curves, then our discovery of 38 PCEBs would imply a total number of PCEBs in the photometric sample of  $\sim 280$ , or  $\sim 14\%$  of the sample. This increases to  $\sim 17\%$  if we take into account the expected non-WDMS contamination. This is consistent with the results from the spectroscopic sample, considering the earlier spectral types within the photometric sample.

### 5.3 The periods of the ellipsoidal modulation systems

There is an interesting clustering of the periods in Table 3, where 11 of the 22 systems have periods between 4–4.5 hours (0.166–0.188 days) and spectral types of mostly M2–3. This is the expected period for stars of this spectral type to fill their Roche-lobes (Baraffe et al. 1998), but is slightly shorter than the periods of cataclysmic variables (CVs) containing stars of this spectral type (Knigge et al. 2011), since they are driven slightly out of thermal equilibrium by mass loss. Hence these systems are most likely pre-CVs, right on the verge of starting mass transfer.

The high percentage of systems within this narrow period range (50% of the ellipsoidal systems) is somewhat surprising. However, given that the photometric sample appears to be dominated by main-sequence stars with M2–3 spectral types, and that ellipsoidal systems are easier to detect the closer they are to Roche-

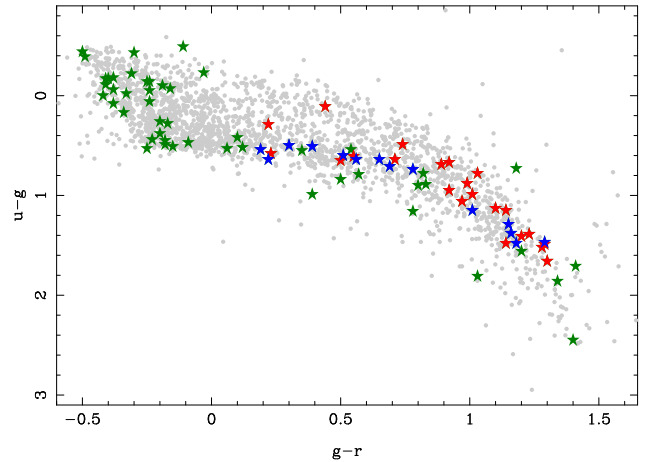


**Figure 8.** Distribution of all spectroscopic WDMS binaries (grey points) in the  $(u - g, g - r)$  colour plane. Previously discovered eclipsing PCEBs are shown in green and generally contain hotter white dwarfs and late-type main-sequence stars and are hence towards the bluer end of the distribution. The 14 newly discovered eclipsing PCEBs from this paper are shown in blue and those systems we found showing large ellipsoidal modulation are shown in red. Both these distributions have redder colours than the known eclipsing systems, indicative of their cooler white dwarfs and/or earlier spectral type main-sequence stars.

lobe filling (see the previous section and Figure 9), this is the most likely period range in which to detect these systems. At shorter periods they have become CVs, whilst at longer periods the ellipsoidal amplitude is too low to detect within the CSS photometry.

### 5.4 Notes on individual systems

#### 5.4.1 SDSS J101356.32+272410.6

This system is one of the handful of new DR 8 spectroscopic systems in our sample and as such has an SDSS spectrum which has been decomposed and fitted to determine the stellar parameters (see Rebassa-Mansergas et al. 2007 for a detailed explanation). The fit yields a massive white dwarf ( $1.14M_{\odot}$ , Rebassa-Mansergas et al. 2012), which would be one of the most massive in an eclipsing



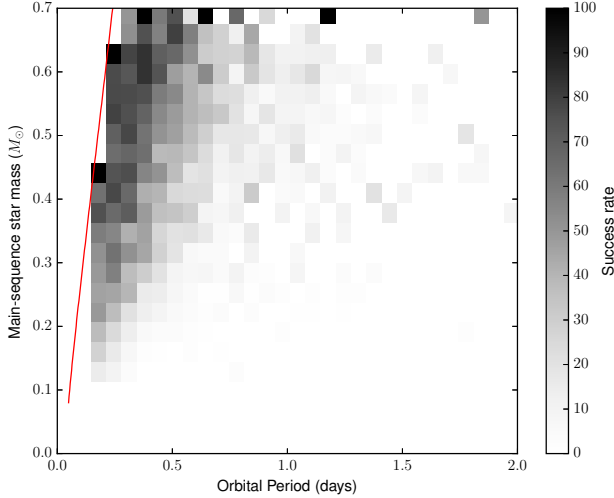


**Figure 9.** The chance of detecting a PCEB (success rate, see Section 5.2) as a function of orbital period and main-sequence star mass. The red line shows where stars fill their Roche-lobes. Unsurprisingly, systems closer to Roche-lobe filling are more likely to be detected.

PCEB. However, as noted by Parsons et al. (2013b) the white dwarf parameters determined from SDSS spectra may not be reliable if the spectrum is dominated by the main-sequence star’s features. Nevertheless, our high-speed eclipse light curve (Figure 3) shows that the ingress and egress are very sharp, implying that the white dwarf is quite small and could therefore be quite massive.

#### 5.4.2 SDSS J112308.40-115559.3

Like SDSS J101356.32+272410.6 this system has an SDSS spectrum which implies that the white dwarf is also massive ( $1.1M_{\odot}$ , Rebassa-Mansergas et al. 2012). The follow up photometry (Figure 3) also revealed a fairly rapid ingress and egress (hence small white dwarf) and so the high mass is possible. However, this white dwarf is also fairly cool ( $T_{\text{eff}} = 10073 \text{ K}$ ), which would make it small almost regardless of the mass. Spectroscopic follow up is required to properly determine the physical parameters of the system.

#### 5.4.3 SDSS J220504.51-062248.4

The spectroscopic fit to the main-sequence star in this system gives a robust spectral type of M2. However, given the period of 3.1 h we would expect such a star to fill its Roche-lobe. There is no sign of this spectroscopically and the CSS light curve shows very little out of eclipse variation, implying that the system is not close to Roche-lobe filling. This also rules out an M2 subdwarf, since even with a higher density the system would still be very close to Roche-lobe filling. This system was observed with ULTRACAM in the  $u'$ ,  $g'$  and  $r'$  bands and showed that the object being eclipsed was bluer (hence hotter) than the M star, since the eclipse was deeper in the shorter wavelength bands. This, combined with the Galaxy Evolution Explorer (GALEX) magnitudes strongly imply that the eclipse is of a white dwarf by a low-mass star. However, We suspect that this system may in fact be a triple system with a white dwarf in a close, eclipsing binary with a so-far undetected low-mass star and with a wide M2 companion. Alternately, the M2 star may just lie along the line of sight to the binary.

#### 5.4.4 SDSS J234035.84+185555.0

This system contains a main-sequence star of M1 spectral type, making it one of the more massive main-sequence stars in an eclipsing PCEB. Only the K2 star in V471 Tau (O’Brien et al. 2001) and the G5 star in KOI-3278 (Kruse & Agol 2014) are more massive. Stars of this mass often show strong disagreement between their measured physical parameters (e.g. radii, temperature) and theoretical predictions (López-Morales 2007) making this a useful system for investigating this issue.

## 6 CONCLUSIONS

We have combined a catalogue of photometrically selected white dwarf plus main-sequence binaries from the Sloan Digital Sky Survey with the long-term photometric data of the Catalina Sky Surveys in order to identify new close post common-envelope binaries and specifically those that are eclipsing. We have identified 17 eclipsing systems, of which 14 were previously unknown, as well as 3 candidate eclipsing systems and 22 other close binaries. We have presented follow-up photometry and spectroscopy for many of these in order to better characterise their component stars.

The newly discovered close binaries generally contain early M-type main-sequence stars, that are underrepresented in the SDSS spectroscopic white dwarf main-sequence star sample. These partially convective systems, in combination with the spectroscopic white dwarf main-sequence star sample, will offer valuable information on the angular momentum loss and evolution of close binaries as well as constraining the mass-radius relationship of white dwarfs and low-mass main-sequence stars.

## ACKNOWLEDGMENTS

We thank the referee for useful comments and suggestions. SGP acknowledges financial support from FONDECYT in the form of grant number 3140585. ULTRACAM, VSD and SPL are supported by the Science and Technology Facilities Council (STFC). TRM and EB were supported the STFC #ST/L000733/1. The research leading to these results has received funding from the European Research Council under the European Union’s Seventh Framework Programme (FP/2007-2013) / ERC Grant Agreement n. 320964 (WDTracer). MRS thanks for support from FONDECYT (1141269) and Millennium Science Initiative, Chilean ministry of Economy: Nucleus RC130007. ARM acknowledges financial support from the Postdoctoral Science Foundation of China (grants 2013M530470 and 2014T70010) and from the Research Fund for International Young Scientists by the National Natural Science Foundation of China (grant 11350110496). We also acknowledge the travel support provided by the Royal Society. This work has made use of data obtained at the Thai National Observatory on Doi Inthanon, operated by NARIT.

## REFERENCES

- Abazajian, K. N., et al., 2009, *ApJS*, 182, 543
- Adelman-McCarthy, J. K., et al., 2008, *ApJS*, 175, 297
- Almenara, J. M., et al., 2012, *MNRAS*, 420, 3017
- Backhaus, U., et al., 2012, *A&A*, 538, A84
- Baraffe, I., Chabrier, G., 1996, *ApJ*, 461, L51

- Baraffe, I., Chabrier, G., Allard, F., Hauschildt, P. H., 1998, *A&A*, 337, 403
- Becker, A. C., Bochanski, J. J., Hawley, S. L., Ivezić, Ž., Kowalski, A. F., Sesar, B., West, A. A., 2011, *ApJ*, 731, 17
- Beuermann, K., Dreizler, S., Hessman, F. V., Deller, J., 2012a, *A&A*, 543, A138
- Beuermann, K., et al., 2010, *A&A*, 521, L60
- Beuermann, K., et al., 2012b, *A&A*, 540, A8
- Copperwheat, C. M., Marsh, T. R., Dhillon, V. S., Littlefair, S. P., Hickman, R., Gänsicke, B. T., Southworth, J., 2010, *MNRAS*, 402, 1824
- Dhillon, V. S., et al., 2007, *MNRAS*, 378, 825
- Dhillon, V. S., et al., 2014, *MNRAS*, 444, 3504
- Drake, A. J., et al., 2009, *ApJ*, 696, 870
- Drake, A. J., et al., 2010, *ArXiv e-prints*
- Drake, A. J., et al., 2014a, *ApJS*, 213, 9
- Drake, A. J., et al., 2014b, *ApJ*, 790, 157
- Gänsicke, B. T., Araujo-Betancor, S., Hagen, H.-J., Harlaftis, E. T., Kitsionas, S., Dreizler, S., Engels, D., 2004, *A&A*, 418, 265
- Ivanova, N., et al., 2013, *A&A Rev.*, 21, 59
- Kleinman, S. J., et al., 2004, *ApJ*, 607, 426
- Knigge, C., Baraffe, I., Patterson, J., 2011, *ApJS*, 194, 28
- Kovács, G., Zucker, S., Mazeh, T., 2002, *A&A*, 391, 369
- Kruse, E., Agol, E., 2014, *Science*, 344, 275
- Law, N. M., et al., 2012, *ApJ*, 757, 133
- Li, L., Zhang, F., Han, Q., Kong, X., Gong, X., 2014, *MNRAS*, 445, 1331
- Littlefair, S. P., et al., 2014, *ArXiv e-prints*
- López-Morales, M., 2007, *ApJ*, 660, 732
- Marsh, T. R., et al., 2014, *MNRAS*, 437, 475
- Maxted, P. F. L., Marsh, T. R., Morales-Rueda, L., Barstow, M. A., Dobbie, P. D., Schreiber, M. R., Dhillon, V. S., Brinkworth, C. S., 2004, *MNRAS*, 355, 1143
- Maxted, P. F. L., O'Donoghue, D., Morales-Rueda, L., Napiwotzki, R., Smalley, B., 2007, *MNRAS*, 376, 919
- Morales, J. C., Gallardo, J., Ribas, I., Jordi, C., Baraffe, I., Chabrier, G., 2010, *ApJ*, 718, 502
- Muirhead, P. S., et al., 2013, *ApJ*, 767, 111
- Nebot Gómez-Morán, A., et al., 2011, *A&A*, 536, A43
- O'Brien, M. S., Bond, H. E., Sion, E. M., 2001, *ApJ*, 563, 971
- O'Connell, D. J. K., 1951, *Publications of the Riverview College Observatory*, 2, 85
- O'Donoghue, D., Koen, C., Kilkenney, D., Stobie, R. S., Koester, D., Bessell, M. S., Hambly, N., MacGillivray, H., 2003, *MNRAS*, 345, 506
- Parsons, S. G., Marsh, T. R., Copperwheat, C. M., Dhillon, V. S., Littlefair, S. P., Gänsicke, B. T., Hickman, R., 2010a, *MNRAS*, 402, 2591
- Parsons, S. G., Marsh, T. R., Gänsicke, B. T., Schreiber, M. R., Bours, M. C. P., Dhillon, V. S., Littlefair, S. P., 2013a, *MNRAS*, 436, 241
- Parsons, S. G., et al., 2010b, *MNRAS*, 407, 2362
- Parsons, S. G., et al., 2012a, *MNRAS*, 420, 3281
- Parsons, S. G., et al., 2012b, *MNRAS*, 426, 1950
- Parsons, S. G., et al., 2012c, *MNRAS*, 419, 304
- Parsons, S. G., et al., 2013b, *MNRAS*, 429, 256
- Pyrzas, S., et al., 2009, *MNRAS*, 394, 978
- Pyrzas, S., et al., 2012, *MNRAS*, 419, 817
- Rebassa-Mansergas, A., Gänsicke, B. T., Rodríguez-Gil, P., Schreiber, M. R., Koester, D., 2007, *MNRAS*, 382, 1377
- Rebassa-Mansergas, A., Nebot Gómez-Morán, A., Schreiber, M. R., Girven, J., Gänsicke, B. T., 2011, *MNRAS*, 413, 1121
- Rebassa-Mansergas, A., Nebot Gómez-Morán, A., Schreiber, M. R., Gänsicke, B. T., Schwöpe, A., Gallardo, J., Koester, D., 2012, *MNRAS*, 419, 806
- Rebassa-Mansergas, A., Agurto-Gangas, C., Schreiber, M. R., Gänsicke, B. T., Koester, D., 2013a, *MNRAS*, 433, 3398
- Rebassa-Mansergas, A., Schreiber, M. R., Gänsicke, B. T., 2013b, *MNRAS*, 429, 3570
- Ren, J. J., et al., 2014, *A&A*, 570, A107
- Scargle, J. D., 1982, *ApJ*, 263, 835
- Schreiber, M. R., et al., 2010, *A&A*, 513, L7
- Schwarzenberg-Czerny, A., 1996, *ApJ*, 460, L107
- Steele, I. A., Bates, S. D., Gibson, N., Keenan, F., Meaburn, J., Mottram, C. J., Pollacco, D., Todd, I., 2008, in *Proc. SPIE*, vol. 7014, p. 70146J
- Stellingwerf, R. F., 1978, *ApJ*, 224, 953
- Tappert, C., Gänsicke, B. T., Schmidtobreick, L., Aungwerojwit, A., Mennickent, R. E., Koester, D., 2007, *A&A*, 474, 205
- van den Besselaar, E. J. M., et al., 2007, *A&A*, 466, 1031
- Webbink, R. F., 1984, *ApJ*, 277, 355
- Willems, B., Kolb, U., 2004, *A&A*, 419, 1057
- York, D. G., et al., 2000, *AJ*, 120, 1579
- Zorotovic, M., Schreiber, M. R., Gänsicke, B. T., Nebot Gómez-Morán, A., 2010, *A&A*, 520, A86
- Zorotovic, M., Schreiber, M. R., Gänsicke, B. T., 2011, *A&A*, 536, A42

#### APPENDIX A: ECLIPSING WHITE DWARF PLUS MAIN-SEQUENCE / BROWN DWARF BINARIES

**Table A1.** Detached, eclipsing white dwarf plus main-sequence / brown dwarf binaries. Our newly discovered systems are highlighted in bold. See Marsh et al. (2014) for an explanation of the timing system used for T0, the mid-eclipse time. References: (1) This paper, (2) Law et al. (2012), (3) Kleinman et al. (2004), (4) Pyrzas et al. (2009), (5) Parsons et al. (2012b), (6) Becker et al. (2011), (7) Parsons et al. (2013a), (8) Drake et al. (2014a), (9) O’Brien et al. (2001), (10) Maxted et al. (2007), (11) Parsons et al. (2013b), (12) Drake et al. (2010), (13) Parsons et al. (2012c), (14) Drake et al. (2014b), (15) Pyrzas et al. (2012), (16) Parsons et al. (2012a), (17) van den Besselaar et al. (2007), (18) O’Donoghue et al. (2003), (19) Littlefair et al. (2014), (20) Parsons et al. (2010a), (21) Muirhead et al. (2013), (22) Kruse & Agol (2014), (23) Almenara et al. (2012), (24) Maxted et al. (2004).

Name	RA	Dec	Period (Days)	T0 BMJD(TDB)	WD mass ( $M_{\odot}$ )	WD $T_{\text{eff}}$ (K)	MS star sp type	$r$ mag	Ref
<b>SDSS J0023+1348</b>	00:23:48.75	+13:48:06.1	0.353930(5)	54733.2550(10)				18.2	1
<b>SDSS J0024+1745</b>	00:24:12.87	+17:45:31.4	0.2000379(5)	56482.19681(9)				17.6	1
PTFEB11.441	00:45:46.00	+41:50:30.0	0.35871(5)	55437.8165(1)	0.54	8500	M3	16.4	2
SDSS J0106-0014	01:06:22.99	-00:14:56.2	0.08501533140(2)	55059.056102(2)	0.37	14393	M8	18.4	3
SDSS J0110+1326	01:10:09.09	+13:26:16.1	0.3326867540(2)	53993.949088(1)	0.47	25900	M4	16.9	4
SDSS J0138-0016	01:38:51.54	-00:16:21.6	0.072764956(5)	55867.007405(7)	0.529	3570	M5	17.4	5
PTFEB28.235	01:52:56.60	+38:44:13.4	0.38612033(3)	55459.60923(7)	0.6	8000	M3	16.6	2
PTFEB28.852	01:55:24.70	+37:31:53.8	0.46152(9)	55530.2335(1)	0.49	8500	M2	17.2	2
SDSS J0259-0044	02:59:53.33	-00:44:00.2	0.144183554(33)	51819.4150(10)			M3	19.3	6
SDSS J0303+0054	03:03:08.35	+00:54:44.1	0.1344376668(1)	53991.117307(2)	0.839	8000	M4.5	18.1	7
SDSS J0308-0054	03:08:56.55	-00:54:50.7	0.18595942(1)	56181.14358(3)			M4.5	17.4	6
CSS J0314+0206	03:14:52.11	+02:06:07.1	0.305296755(4)	56195.206350(2)				17.4	8
CSS J0344+0930	03:44:20.14	+09:30:07.1	0.28066299(1)	56328.1540(5)				18.2	8
V471 Tau	03:50:24.97	+17:14:47.4	0.52118343117(8)	54027.953026(1)	0.84	34500	K2	9.4	9
<b>SDSS J0420+3337</b>	04:20:12.78	+33:37:39.7	0.2205602(5)	56721.890778(2)				16.9	1
RR Cae	04:21:05.53	-48:39:08.3	0.30370368162(5)	51522.5484387(5)	0.44	7540	M5	14.3	10
SDSS J0745+2631	07:45:48.63	+26:31:23.4	0.21926417(8)	53387.2495(10)			M2	17.4	11
SDSS J0821+4559	08:21:45.27	+45:59:23.4	0.50909205(5)	55989.038796(23)	0.66	80938	M2	17.6	11
CSS 40190	08:38:45.86	+19:14:16.5	0.130112321(1)	53469.21993(3)	0.5	11062	M7	18.4	12
SDSS J0857+0342	08:57:46.18	+03:42:55.3	0.0650965381(2)	55552.7127649(7)	0.514	37400	M8	18.3	13
CSS 080502	09:08:12.04	+06:04:21.2	0.1494380537(5)	53466.33317(4)	0.35	17505	M4	17.3	12
LP 486-53	09:08:26.18	+12:36:48.9	0.13919939(1)	54140.3160(5)				16.5	14
SDSS J0927+3329	09:27:41.73	+33:29:59.1	2.308227(1)	56074.906137(21)	0.59	27111	M3	18.2	11
CSS J0935+2700	09:35:08.00	+27:00:49.2	0.20103360(2)	56602.839467(8)				16.6	14
CSS 38094	09:39:47.95	+32:58:07.3	0.330989669(3)	55587.308818(8)	0.49	28442	M5	18.0	12
SDSS J0946+2030	09:46:34.49	+20:30:03.4	0.25286147(5)	56032.94559(3)	0.62	10307	M5	18.9	11
CSS 41631	09:57:19.24	+23:42:40.7	0.150870774(1)	55548.357087(2)	0.43	25891	M2	18.1	12
SDSS J0957+3001	09:57:37.59	+30:01:36.5	1.926125(1)	56014.975114(32)	0.42	28064	M3	18.8	11
<b>SDSS J1013+2724</b>	10:13:56.32	+27:24:10.6	0.129040379(4)	56280.182901(8)	1.14	15601	M4	17.2	1
SDSS J1021+1744	10:21:02.25	+17:44:39.9	0.14035862(3)	56093.9055(1)	0.5	32595	M4	19.0	11
SDSS J1028+0931	10:28:57.78	+09:31:29.8	0.235025695(6)	56001.093511(9)	0.42	18756	M3	15.6	11
SDSS J1057+1307	10:57:56.93	+13:07:03.5	0.125162238(3)	56010.062214(14)	0.34	12536	M5	18.6	11
<b>SDSS J1123-1155</b>	11:23:08.40	-11:55:59.3	0.7691358(14)	56685.789599(9)	1.26	10073	M5	17.5	1
SDSS J1210+3347	12:10:10.13	+33:47:22.9	0.124489764(1)	54923.033686(6)	0.415	6000	M5	16.2	15
SDSS J1212-0123	12:12:58.25	-01:23:10.2	0.335870942(4)	54104.20914(2)	0.439	17900	M4	16.9	16
SDSS J1223-0056	12:23:39.61	-00:56:31.1	0.0900784(13)	55707.016987(2)	0.45	11565	M6	18.0	11
CSS 25601	12:44:32.25	+10:17:10.8	0.22785631(9)	53466.3611(11)	0.37	21168	M5	18.3	12
SDSS J1307+2156	13:07:33.49	+21:56:36.7	0.21632224(1)	56007.22137(2)			M4	17.4	11
CSS 21616	13:25:18.18	+23:38:07.9	0.194958992(2)	55653.454186(9)				18.3	12
DEC Vn	13:26:53.26	+45:32:46.7	0.3641393156(5)	52784.054043(1)	0.51	8000	M3	12.5	17
SDSS J1329+1230	13:29:25.21	+12:30:25.4	0.080966255(1)	55271.054818(1)	0.35	13000	M8	17.5	11
WD 1333+005	13:36:16.05	+00:17:31.9	0.1219587642(7)	55611.47667(2)		6000	M5	17.1	12
CSS 21357	13:48:41.61	+18:34:10.5	0.248431787(2)	56000.161910(7)	0.59	15071	M4	17.2	12
QS Vir	13:49:51.95	-13:13:37.5	0.150757612(1)	48689.13553(5)	0.77	14085	M3	14.1	18
SDSS J1408+2950	14:08:47.14	+29:50:44.9	0.19179048(4)	53506.2885(5)	0.49	29050	M5	19.0	11
CSS 07125	14:10:57.73	-02:02:36.7	0.36349709(2)	53464.48862(24)	0.38	29268	M4	18.9	12
CSS 21055	14:11:26.20	+20:09:11.1	0.0845327526(13)	55991.388717(2)	0.53	13000	L7	18.0	19
SDSS J1411+1028	14:11:34.70	+10:28:39.7	0.16750961(3)	56031.17278(5)	0.36	30419	M3	19.2	11
<b>SDSS J1411+2117</b>	14:11:50.74	+21:17:50.0	0.3216383(1)	56396.117096(24)			M3	16.4	1
GK Vir	14:15:36.41	+01:17:18.2	0.3443308387(1)	42543.337714(3)	0.563	55000	M4.5	17.3	16
<b>SDSS J1417+0801</b>	14:17:24.36	+08:01:12.0	0.23918209(5)	56826.97958(1)				18.6	1
CSS 080408	14:23:55.06	+24:09:24.3	0.382004302(6)	53470.39959(4)	0.4	32595	M5	17.9	12
<b>SDSS J1424+1124</b>	14:24:27.69	+11:24:57.9	0.2392937(1)	56391.123610(8)				17.1	1
SDSS J1435+3733	14:35:47.87	+37:33:38.5	0.1256310520(3)	54148.204447(3)	0.505	12500	M5	17.3	4
CSS 09797	14:56:34.30	+16:11:37.7	0.2291202(2)	51665.7893(30)	0.34	19149	M5	18.0	12
<b>SDSS J1540+3705</b>	15:40:57.27	+37:05:43.4	0.26143467(5)	56434.18457(3)			M4	16.8	1

Name	RA	Dec	Period (Days)	T0 BMJD(TDB)	WD mass ( $M_{\odot}$ )	WD $T_{\text{eff}}$ (K)	MS star sp type	$r$ mag	Ref
SDSS J1548+4057	15:48:46.00	+40:57:28.8	0.185515281(1)	54592.07295(3)	0.646	11700	M6	18.4	4
NN Ser	15:52:56.20	+12:54:47.2	0.1300801218(1)	47344.0254693(7)	0.535	57000	M4	16.9	20
<b>SDSS J1642-0634</b>	16:42:35.97	-06:34:39.7	0.28689(1)	56770.19243(3)				17.1	1
CSS J1653+3914	16:53:52.40	+39:14:10.3	0.21981035(1)	54919.4450(5)				16.5	14
KOI-256	19:00:44.43	+49:33:55.3	1.3786548(1)	55373.824838(1)	0.592	7100	M3	15.8	21
KOI-3278	19:26:05.97	+38:27:21.1	88.18052(27)	55084.9190(23)	0.634	9960	G5	14.6	22
2MASS J1942+4745	19:42:37.20	+47:45:48.5	0.350468722(6)	53589.93613(1)	0.61	20470	M4	18.7	23
RX J2130.6+4710	21:30:18.60	+47:10:08.0	0.5210361666(1)	52785.1827943(5)	0.554	18000	M3.5	14.2	24
CSS J2131+0758	21:31:02.61	+07:58:10.1	0.24789997(5)	54730.2735(5)				18.5	8
<b>SDSS J2205-0622</b>	22:05:04.51	-06:22:48.4	0.132386898(4)	56178.079537(3)			M2	17.1	1
CSS 09704	22:08:23.66	-01:15:34.1	0.156505698(1)	53507.45739(2)	0.37	29302	M4	18.8	12
SDSS J2235+1428	22:35:30.61	+14:28:55.1	0.144456765(1)	55469.065472(6)	0.45	21045	M4	18.8	11
<b>SDSS J2306-0555</b>	23:06:27.54	-05:55:33.2	0.20008319(6)	57024.53910(2)				16.2	1
<b>SDSS J2327+2119</b>	23:27:05.33	+21:19:42.1	0.84974077(5)	54363.2180(10)			M4	17.8	1
<b>SDSS J2340+1855</b>	23:40:35.84	+18:55:55.0	0.30765754(5)	54977.4535(10)			M1	17.2	1